# Numerical study of laminar starting forced plumes at high Schmidt number

Huong Lan Tran, Anne Sergent, Gilles Bernard-Michel, Patrick Le Quere

▶ **To cite this version:**

Huong Lan Tran, Anne Sergent, Gilles Bernard-Michel, Patrick Le Quere. Numerical study of laminar starting forced plumes at high Schmidt number. CFM 2013 - 21ème Congrès Français de Mécanique, Aug 2013, Bordeaux, France. hal-03439815

**HAL Id: hal-03439815**
**https://hal.science/hal-03439815**

Submitted on 22 Nov 2021

**HAL** is a multi-disciplinary open access archive for the deposit and dissemination of scientific research documents, whether they are published or not. The documents may come from teaching and research institutions in France or abroad, or from public or private research centers.

L'archive ouverte pluridisciplinaire **HAL**, est destinée au dépôt et à la diffusion de documents scientifiques de niveau recherche, publiés ou non, émanant des établissements d'enseignement et de recherche français ou étrangers, des laboratoires publics ou privés.

# Numerical study of laminar starting plumes at high Schmidt number

**H.-L. Tran[a,b], A. Sergent[a,c], G. Bernard-Michel[b], P. Le Quéré[a]**

a. *LIMSI-CNRS, UPR 3251, 91403 Orsay cedex*
b. *CEA Saclay, DEN/DM2S/STMF/LIEFT 91191 Gif sur Yvette Cedex*
c. *UPMC Paris 06, 75005 Paris*

## Résumé :

*On considère un mélange binaire isotherme glycérol-eau (pour des nombres de Schmidt allant de* $6 \cdot 10^4$ *à* $6 \cdot 10^5$*) remplissant un réservoir où un mélange binaire plus léger est injecté au centre de la paroi inférieure. La propagation d'un panache forcé axisymétrique est modélisée numériquement pour des nombres de Grashof compris entre* $10^5$ *et* $10^7$ *et des nombres de Reynolds d'injection entre* $0.3 - 12$*. On se place dans la configuration expérimentale de [6]. Les panaches se développent à une vitesse d'ascension constante après une courte période initiale d'accélaration. Globalement un bon accord est obtenu vis-à-vis des résultats expérimentaux, aussi bien en ce qui concerne la vitesse d'ascension que les caractéristiques de la tête des panaches (type et dimensions). Une corrélation entre la vitesse d'ascension et un nombre de Reynolds modifié est cependant proposé pour tenir compte de la différence de viscosité des deux fluides.*

## Abstract :

*We consider an isothermal binary mixture of glycerol-water for Schmidt numbers around* $6 \cdot 10^4 - 6 \cdot 10^5$ *filling a tank where a light binary mixture is injected in the center of the bottom wall. The propagation of an axisymmetrical buoyant-jet is modeled numerically for Grashof numbers in the range of* $10^5 - 10^7$ *and injection Reynolds numbers in the range of* $0.3 - 12$*. The studied configuration corresponds to the experimental set-up of [6]. In agreement with experimental data, the plume reaches a constant ascent velocity after a short initial period of acceleration. Two types of plume head are obtained numerically. Basically a good agreement with the experiment has been found concerning the ascent velocity value as well as the head shape (type and size). A modified scaling law of the ascent velocity versus a modified Reynolds number is proposed to take into account the difference of kinetic viscosity of both fluids.*

## Mots clefs : **buoyant jet, glycerol-water mixture, mass plume, starting plume**

## 1 Introduction

This work deals with the convection of a binary mixture of glycerol-water in an isothermal enclosure at constant pressure. We focus here on laminar forced compositionally buoyant plumes generated by a local injection of a buoyant fluid into an ambient quiescent heavier fluid. Most of the previous theoretical or experimental works concerning starting plumes have been done for thermal plumes (see for example [1, 4, 5, 7, 8]), studying the morphology of the plumes and establishing scaling laws for their ascent velocity or the shape of plume heads. A similar study has been carried out experimentally for plumes driven by compositional difference at high Schmidt numbers [6]. A few comparison exercises between experimental and numerical models which exist in the literature concern thermal plumes [7, 8]. Therefore the present study aims at establishing a numerical modelling for compositional buoyant plumes by using a comparison exercise with experimental data of [6].

In the next section, the problem formulation as well as the numerical methods are described. Then

results for the ascent velocity (and the corresponding scaling laws) and head morphologies are presented.

# 2 Problem model and numerical methods

## 2.1 Physical configuration

We consider a laminar starting plume of a light glycerol-water mixture injected by a circular inlet of 3.0 mm of diameter ($d_i$) into a cylindrical tank of 50.2 cm height ($L_z$) and of diameter equal to 15.2 cm, filled with a heavy glycerol-water mixture. The top of the tank is a free surface. This configuration aims to mimic the experimental apparatus of [6], insofar as the geometry for the computational domain has the same cross-sectional area as that in the experiment.

At the initial state, the ambient fluid filling the cavity is quiescent and of constant density $\rho_a$. The light fluid is injected at a constant density $\rho_i$ and constant flow rate $Q$. As the typical time of injection is around 30 seconds and the largest flow rate equal to $Q = 0.4mL/s$, the total injected volume is small enough to consider the increase of the fluid level in the tank negligible.

Dimensionless parameters can be defined : the injection Reynolds number ($Re_i = \frac{4Q}{\pi\nu_i d_i}$), the Grashof number ($Gr = \frac{g\Delta\rho L_z^3}{\rho_a\nu_a^2}$, with $\Delta\rho = \rho_a - \rho_i$), the Schmidt numbers of the ambient and injected fluids ($Sc_a = \frac{\nu_a}{D_a}$ and $Sc_i = \frac{\nu_i}{D_i}$), where $\rho$ is the density, $\nu$ the dynamic viscosity, $g$ the gravity and $D$ the diffusion coefficient. The subscripts $a$ and $i$ refer respectively to the ambient and injected fluids.

In accordance with the experimental study[6], several test-cases with different mixtures of glycerol and water are investigated. They are defined by the composition of the ambient and injected mixtures (i.e. the Schmidt numbers) and the mass flow rate injected in the cavity (i.e. the injection Reynolds number). The corresponding physical properties of the fluids and the relative dimensionless parameters are listed respectively in tables 1 and 2. The pure water (referred by the subscript 2) and pure glycerol (referred by the subscript 1) density and dynamic viscosities depend only on the temperature (formula from [2]). They are estimated at $21°C$, in agreement with the experiment. The mixture physical properties (diffusion and viscosity) depends on the mass fraction of one of the components and are estimated at the same temperature (see [2] and [3] for more details).

As seen in table 2, the Schmidt numbers of the mixtures are very high. Consequently, the flow can be considered to be incompressible.

| Cases | $\rho_i$ $[kg/m^3]$ | $Y_{1i}$ | $\rho_a$ $[kg/m^3]$ | $Y_{1a}$ | $\frac{\Delta\rho}{\rho_a}$ | $\nu_i$ $[m^2/s]$ | $\nu_a$ $[m^2/s]$ |
|---|---|---|---|---|---|---|---|
| D1 | 1174.5 | 0.6656 | 1177.54 | 0.6771 | 0.00258 | $14.19 \cdot 10^{-6}$ | $15.47 \cdot 10^{-6}$ |
| D2 | 1175.2 | 0.6683 | 1179.7 | 0.6852 | 0.00381 | $14.47 \cdot 10^{-6}$ | $16.48 \cdot 10^{-6}$ |
| D4 | 1204.5 | 0.7786 | 1215.95 | 0.8218 | 0.00942 | $37.87 \cdot 10^{-6}$ | $60.32 \cdot 10^{-6}$ |
| D5 | 1213.5 | 0.8215 | 1216.055 | 0.8223 | 0.00210 | $54.32 \cdot 10^{-6}$ | $60.59 \cdot 10^{-6}$ |

TABLE 1 – Physical properties of the test-cases. $Y_1$ is the mass fraction of glycerol.

| Case | $Sc_a$ | $Sc_i$ | $Gr$ |
|---|---|---|---|
| D1 | 64128 | 55805 | $1.324 \cdot 10^7$ |
| D2 | 70976 | 57598 | $1.743 \cdot 10^7$ |
| D4 | 592574 | 274688 | $2.755 \cdot 10^6$ |
| D5 | 597078 | 498085 | $8.2 \cdot 10^5$ |

TABLE 2 – Dimensionless parameters of the simulated test cases.

## 2.2 Governing equations

We solve the 2D axisymmetrical equations for the incompressible flow of a binary mixture in a cavity. The equations are made dimensionless by the following reference quantities : the average injection velocity ($\overline{U} = 4Q/\pi d_i^2$), the cavity height ($L_z$) and the ambient physical properties ($\rho_a$, $\nu_a$, $D_a$). The resulting dimensionless set of equations are

$$\nabla \cdot \mathbf{u} = 0 \quad (1)$$

$$\frac{\partial \rho Y_1}{\partial t} + \nabla \cdot (\rho Y_1 \mathbf{u}) = \frac{1}{ReSc_a} \nabla \cdot (\rho D \nabla Y_1) \quad (2)$$

$$\frac{\partial \rho \mathbf{u}}{\partial t} + \nabla \cdot (\rho \mathbf{u} \otimes \mathbf{u}) = -\nabla p + \frac{1}{Re} \nabla \cdot (\rho \nu (\nabla \mathbf{u} + \nabla^t \mathbf{u})) + \frac{1}{Fr} \rho \mathbf{z} \quad (3)$$

$$\rho = \rho_1 Y_1 + \rho_2 (1 - Y_1) \quad (4)$$

where $\mathbf{u} = (u_r, u_z)$ stands for the velocity of the mixture, $\rho$ the mixture density and $Y_1$ the glycerol mass fraction. $\mathbf{z}$ is the unit vector oriented in the opposite direction to the gravity. The Reynolds $Re$ and Froude $Fr$ numbers are defined as : $Re = \frac{\overline{U} L_z}{\nu_a}$ and $Fr = \frac{\overline{U}^2}{g L_z}$.

The boundary conditions are the following : at the bottom inlet ($r <= d_i/2$, $z = 0$), a Poiseuille profile is imposed for $\mathbf{u}$ corresponding to a mass flow rate of $Q$. The fluid is injected at a fixed mass fraction $Y_1 = Y_{1i}$. At the top ($z = 1$), we have a free-surface boundary condition for $\mathbf{u}$. On the walls, a no-slip boundary condition is applied. The boundary condition for the glycerol mass fraction corresponds to a Neumann boundary condition for $Y_1$ ($\partial Y_1/\partial z = 0$) applied on all walls and at the top free-surface.

In the initial state, the whole cavity is at rest ($\mathbf{u} = \mathbf{0}$) and the fluid mixture is uniform ($Y_1 = Y_{1a}$).

## 2.3 Numerical methods

We solve the equations (1-4) in the axisymmetrical coordinates using a second-order semi-implicit scheme. It combines a second-order backward differential formula (BDF2) with an implicit treatment for the diffusion terms and an explicit second-order Adams-Bashforth extrapolation for the nonlinear terms. Incompressibility is imposed by a projection method which retains second-order accuracy of the time integration. A finite-volume discretization on staggered grids is used. Second-order central difference scheme is employed for all the spatial derivative terms. The discrete systems resulting from the finite-volume approach are splitted by an ADI technique and then solved through Thomas algorithm, while the Poisson equation for pressure correction is solved by a multigrid method.

A uniform grid has been used in both directions ($e_r, e_z$). The grid convergence has been investigated for two test-cases corresponding to two different types of plume heads : confined head (D4, $Q = 0.4ml/s$) and dispersed head (D2, $Q = 0.267ml/s$). By varying the horizontal mesh from 226 to 898 cells, and the vertical mesh from 1666 to 3748 cells, it has been shown that the global quantities such as the head velocity ($v_h$), the conduit velocity ($v_c$) and the conduit width ($w_c$) are hardly affected by grid refinement. However the local instantaneous plume height ($h$) and especially the head shape ($w_h, l_h$) are more sensitive. As a compromise we select an intermediate mesh (514x1666) which satisfies for the most sensitive quantity ($l_h$) an error inferior to 3% when comparing to the finest grid. The time step is fixed at $10^{-4}$ dimensionless time unit for each cases, whereas computations are performed until the plume reaches a height of around $30cm$. It means during around 20 to 60 seconds, i.e. around 5000 to 25000 time steps.

# 3 Results

We consider axisymmetrical plumes of buoyant fluid which are developping in a tank. A sequence of snapshots is presented in figure 1-a. As the Schmidt numbers are very large, the diffusion of the mass fraction is slow by comparing to the convection. It results in a starting plume consisting of a thin *conduit* connecting the inlet at the bottom to a *head* at its top.

## 3.1 Ascent velocity

The ascent velocity ($v_h$) with which the mass plume propagates, is measured by tracking the time evolution of the front of the plume. It is well-known, in the case of a thermal plume at high Prandtl number (see for example [4]), that this velocity is constant during a large part of the ascent, when the plume is distant from the inlet and the free-surface. It has also been observed experimentally by [6] for high Schmidt numbers as presented on figure 1-b. Our results obtained by computations are also plotted on this figure for several mass flow rate $Q$ in the case **D4**. It can be noted that the numerical modelling predicts lower plumes than experiment. However the ascent velocity is quite well estimated with an error around 2% (table 3). Figure 1-b shows that the discrepancy originates from the acceleration period. The first measuring point is reproduced with accuracy. But the stage where the ascent velocity increases rapidly to the constant value is too long for the numerical modelling. A lack of spatial resolution close to the inlet and in the lower part of the plume conduit may be responsible of the ascent delay.

A scaling law for the ascent velocity ($v_h = 0.63\sqrt{\frac{g\Delta\rho Q}{\rho_a \nu_i}}$) has been proposed by [6] based on an empirical relation relating the plume Richardson number ($Ri = \frac{g\Delta\rho d}{\rho_a v_h^2}$) to the injection Reynolds number :

$$Ri = 3.2 Re_i^{-0.91} \tag{5}$$

This is an extension of previous theoretical and experimental works [1, 4, 5] concerning thermal starting plumes. For the present numerical results, the dependence of Ri on the injection Reynolds number is plotted in figure 2. We remark that the data are neither aligned nor superimposed with the empirical correlation (eq. 5). This is particularly obvious for the **D4** points. It is noticeable that all the cases have a ratio of kinetic viscosities ($\nu_i/\nu_a$) close to 1 except the **D4** case. Indeed the data can be brought together by taking into account the kinetic viscosity of both fluids in a modified Reynolds number ($Re^* = \frac{\nu_i}{\nu_a} Re_i$). Therefore a new correlation can be proposed : $Ri = 3.7(Re^*)^{-0.79}$.

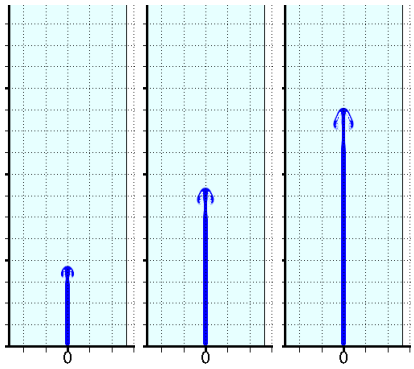

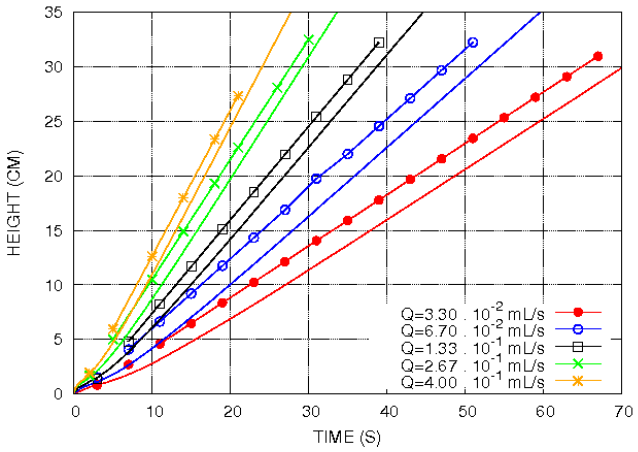


FIGURE 1 – Case **D4** (a) Glycerol mass fraction evolution with an injection rate of $Q = 0.4mL/s$. Each image is $7.2s$ apart. (b) Time evolution of the plume height for $3.3\times10^{-2}\ mL/s \leq Q \leq 4.0\times10^{-1}\ mL/s$, $0.37 \leq Re_i \leq 4.48$. Points-lines are for the experimental data [6] and solid lines are for numerical results.

## 3.2 Shape of plume head

One remarkable feature of the laminar starting mass plume is their head morphology. The head shape can be described by its width $w_h$ and its vertical length $l_h$. Two types of head shape have been found by [6] : the so-called *confined* or *dispersed* heads, which are discriminated by the plume Richardson number. Examples of time evolution of both types of head shape is given in figure 3.

In agreement with experiment [6] we found a confined shape for the case (**D5**, $Q = 0.2mL/s$), which corresponds to the classic "mushroom-shape". This agreement is confirmed by the time evolution of

| $Q(mL/s)$ | $v_h$ (cm/s) | $v_h^e$ (cm/s) | $v_h/v_h^e$ | $Ri$ |
|---|---|---|---|---|
| $3.3 \times 10^{-2}$ | 0.4634 | 0.47 | 0.99 | 12.91 |
| $6.7 \times 10^{-2}$ | 0.6321 | 0.64 | 0.99 | 6.94 |
| $1.33 \times 10^{-1}$ | 0.8461 | 0.86 | 0.98 | 3.87 |
| $2.67 \times 10^{-1}$ | 1.1210 | 1.10 | 1.02 | 2.21 |
| $4.0 \times 10^{-1}$ | 1.3123 | 1.34 | 0.98 | 1.61 |

TABLE 3 – Comparison of the ascent velocities for the case **D4** : numerical simulations ($v_h$) and experimental data ($v_h^e$) extracted from Fig. 2 in [6].

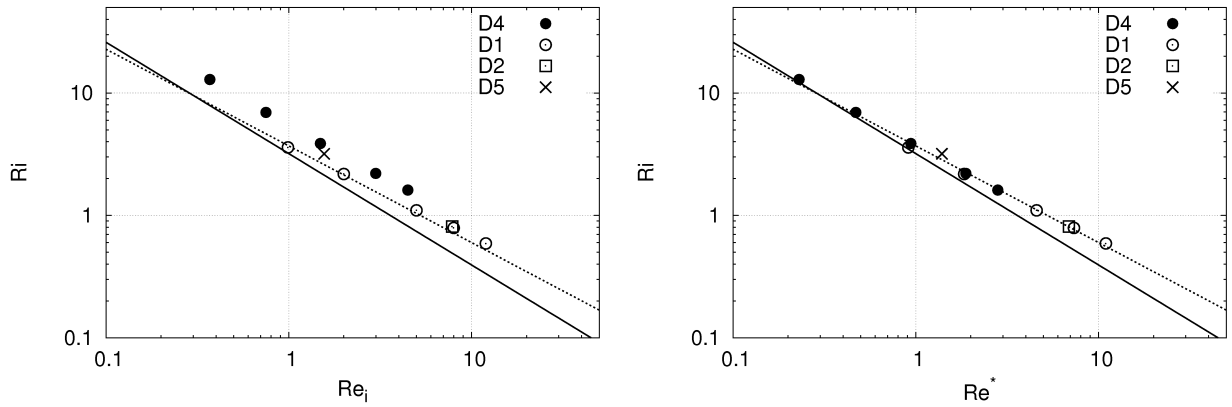


FIGURE 2 – The plume Richardson number as a function of (left) the injection Reynolds number or (right) the modified Reynolds number ($Re^* = \frac{\nu_i}{\nu_a} Re_i$) for 12 plumes. The solid line is $Ri = 3.2 Re_i^{-0.91}$, and the dashed line is $Ri = 3.7 (Re^*)^{-0.79}$.

the head features in the case **D4** presented in a diagram $Re_{hw} - Re_{hl}$ where $Re_{hw} = v_h\, w_h/\nu_i$ and $Re_{hl} = v_h\, l_h/\nu_i$ (see figure 4). Even if the plume heights are slightly smaller than experimental data, a quasi-constant aspect ratio of the head shape $Re_{hw}/Re_{hl}$ is obtained numerically with a value equal to experimental constant of 1.24.

The dispersed head seems to be more difficult to model numerically. The time-evolution of the glycerol mass fraction for the case (**D2**, $Q = 0.267 mL/s$) (fig. 3)exhibits the elongating vertical head length with time. However the instability mechanism of the vortex ring has not been reproduced, perhaps because of a lack of spatial resolution or asymmetry property of the plume as suggested by [6]. Nonetheless the decrease in time of the aspect ratio of the head shape is observed (fig. 4).

## 4 Conclusions

A numerical study of an axisymmetrical laminar starting plume driven by compositional differences has been performed for high Schmidt numbers. The studied configuration corresponds to the experimental set-up of [6]. In agreement with the experimental data, the plume reaches a constant ascent velocity after a short initial period of acceleration. Two types of plume head are obtained numerically. Basically a good agreement with the experiment has been found concerning the ascent velocities as well as the head shape (type, size, aspect ratio). A modified scaling law for the ascent velocity versus a modified Reynolds number is proposed to take into account the difference of kinetic viscosity of the injected and ambient fluids.

However the numerical model fails to predict with accuracy the plume height as well as the shape of dispersed plumes. These discrepancies may originate from a lack of spatial resolution, the difficulties to estimate the physical properties of fluids or differences in the boundary conditions/geometry.

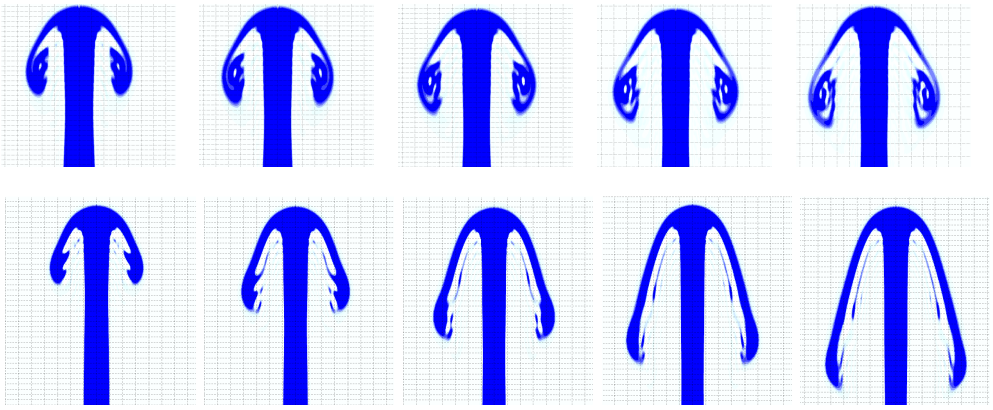

FIGURE 3 – Time evolution of the glycerol mass fraction field. Top : confined heads in case D5 with $Q = 0.2\,mL/s$ ($Re_i = 1.56$, $Ri = 3.19$). Each image is 8.3 s apart. From the first to last image, the size of the head increases from 2.0cmx 2.3 cm to 2.6cmx 2.8 cm. Bottom : dispersed heads in case D2, $Q = 0.267\,mL/s$ ($Re_i = 7.83$, $Ri = 0.81$). Each image is 4.0 s apart. From the first to last image in the sequence, $h$ increases from 10.4 cm to 31.0 cm.

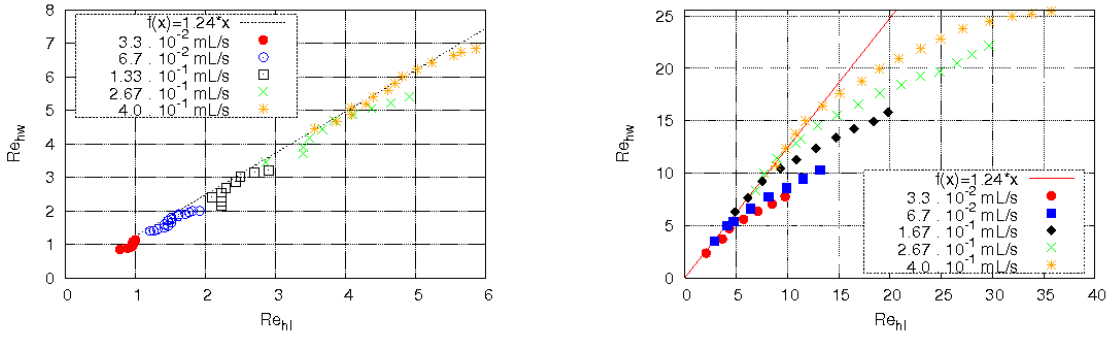


FIGURE 4 – Dimensionless head width $Re_{hw}$ as a function of the dimensionless vertical head length $Re_{lh}$. Left : D4 set of plumes. All of the plume heads in this set are confined. Right : D1 set of plumes. All of the plume heads in this set are dispersed except for the plume with the smallest value of $Q$.

## Références

[1] G. K. Batchelor 1954 Heat convection and buoyancy effects in fluids. *Q. J. R. Met. Soc.* **80** 339

[2] N. S. Cheng 2008 Formula for viscosity of glycerol-water mixture. *Engineering Chemistry Research* **47**

[3] X. He, A. Fowler, and M. Toner 2006 Water activity and mobility in solutions of glycerol and small molecular weight sugars : Implication for cryo- and lyopreservation. *J. Appl. Phys.* **100** 074702

[4] E. Kaminski and C. Jaupart 2003 Laminar starting plumes in high-Prandtl-number fluids. *J. Fluid Mech.* **478** 287–298

[5] E. Moses and C. Zocchi and A. Libchaber 1993 An experimental study of laminar plumes *J. Fluid Mech.* **251** 581

[6] M. C. Rogers and S. W. Morris 2009 Natural versus forced convection in laminar starting plumes. *Phys. Fluids* **21** 083601

[7] P. E. van Keken 1997 Evolution of starting mantle plumes : a comparison between numerical and laboratory models *Earth and Planetary Science Letters* **148** 1-11

[8] J. Vatteville and P. E. van Keken and A. Limare and A. Davaille 2009 Starting laminar plumes : comparison of laboratory and numerical modeling. *Geochem. Geophys. Geosyst.* **10** Q12013